2024 European Control Conference (ECC)
June 25-28, 2024. Stockholm, Sweden

On the effective implementation of control structures to multi-DoF wave energy converters

Maialen Agirre-Aspiazu, Yerai Peña-Sanchez, Demian Garcia-Violini, Ander Zarketa-Astigarraga, Markel Penalba and John V. Ringwood

***Abstract*— Maximising energy output through advanced control strategies is pivotal for the economic viability of wave energy converters (WECs). However, most existing literature primarily focuses on theoretical case studies, where WECs are constrained to operate in a single degree of freedom (DoF). This simplification is made due to the added complexity of optimizing across multiple DoFs. In this study, we assess the necessity of incorporating multiple DoFs within the control framework, evaluating its effectiveness in a numerical simulation environment that replicates WEC performance across multiple DoFs. To provide a basis for comparison, we contrast the conventional PI controller with the innovative LiteCon controller. Our study reveals two key findings: (i) Single DoF control may suffice when the primary DoF of the power take-off system is accurately identified, and (ii) the straightforward LiteCon controller outperforms the traditional PI controller by a significant margin.**

I. Introduction

The energy sector is the largest emitter of greenhouse gases (GHGs) into the atmosphere, being one of the main contributors to climate change. Therefore, the transition towards a carbon-neutral energy system is vital, which entails, on the one hand, a significant reduction of energy consumption and, on the other, a massive implementation of renewable energies [1]. Such an expansion of renewable energies will necessarily require the diversification of renewable sources, including technologies that are still under development, such as marine renewable energies [2]. In this sense, tidal and wave energies are expected to contribute to approximately 10% of the future electricity demand [3], [4].

However, wave energy converters are currently in the early stages of development. Therefore, as of its current stage of advancement, wave power is anticipated to assume a distinct role within the energy landscape. This role encompasses providing energy to remote islands equipped with microgrids, currently reliant on diesel generators for power generation [5], as well as delivering a more dependable, less variable, and highly predictable energy source [6], [7]. Furthermore, in terms of predictability, wave energy holds a comparative advantage when contrasted with other renewable resources [8]. In any case, a significant effort is still required for wave energy to become a real alternative for the niche markets mentioned previously. In this sense, maximising the energy absorption and generation capabilities of wave energy converters (WECs) is one of the key aspects, as highlighted in [9]. Advanced control algorithms can assist in this endeavour [10].

Hence, the primary objective of this study is twofold: (i) to emphasise the significance of distinguishing between the degrees of freedom (DoFs) of the WEC and the power take-off (PTO) system, and (ii) to evaluate the impact of employing a more realistic device model on the assessment of controller's performance. It is important to note that for a 6-DoF floating device that harnesses energy from the relative motion between the buoy and the mooring line, the motion of the PTO is characterized by a combination of all six DoFs of the buoy. However, the vast majority of the studies in the existing literature introduce advanced controllers that assume a simplified single DoF motion (typically heave) for the WEC [11]. However, this assumption may not be accurate when the device motion is not restricted to a single DoF, which is often the case in real devices. By evaluating the controller's performance across different DoFs via a more comprehensive WEC model, this research underscores the importance of using models that are able to represent all the effective DoFs of the WECs when developing control strategies.

The remainder of this paper is organised as follows: Section II introduces the dynamical equation of the WECs, Section III describes the WEC control optimality condition and the considered controller, Section IV proposes a case study, and in Section V the results for such application case are shown. Finally, Section VI draws some conclusions.

II. WEC modelling

In this section, we present the dynamic model of the point absorber WEC, which expresses how the floating body interacts with the fluid (water) and how the different DoFs of the WEC interact with each other. Thus, we formulate this model in the time-domain using Newton's second law as follows:

$$(m + \mu_\infty)\,\ddot{x}(t) = f_{\mathrm{e}}(t) - f_{\mathrm{h}}(t) - f_{\mathrm{r}}(t) - f_{\mathrm{m}}(t) - f_{\mathrm{u}}(t), \quad (1)$$

where the mass matrix, denoted as $m \in \mathbb{R}^{n_{\mathrm{DoF}} \times n_{\mathrm{DoF}}}$, contains the mass/inertia information of the WEC on the different DoFs, while the off-diagonal elements account for interactions and the state vectors $x(t) \in \mathbb{R}^{n_{\mathrm{DoF}}}$, $\dot{x}(t) \in \mathbb{R}^{n_{\mathrm{DoF}}}$ (or equivalently, $v(t)$), and $\ddot{x}(t) \in \mathbb{R}^{n_{\mathrm{DoF}}}$ (or equivalently, $a(t)$) describe the position, velocity, and acceleration of the WEC on the different DoFs, respectively. The forces/torques acting on the WECs, as introduced in Equation (1), include (i) the hydrostatic force, denoted as $f_{\mathrm{h}}(t)$, resulting from buoyancy and gravity forces, which is represented as $S_{\mathrm{h}}x(t)$, with $S_{\mathrm{h}} \in \mathbb{R}^{n_{\mathrm{DoF}} \times n_{\mathrm{DoF}}}$ the hydrostatic stiffness matrix; (ii) the radiation force, originating from waves radiated due to WEC motion, is calculated using a convolution integral as

$f_{\mathrm{r}}(t) = k_{\mathrm{r}_{i,j}}(t) * \dot{x}_j(t)$, with $k_{\mathrm{r}}(t)$ representing the radiation convolution kernel; (iii) the mooring force, modelled as a spring-damper system, is expressed as $f_{\mathrm{m}}(t) = k_{\mathrm{m}}x(t) + b_{\mathrm{m}}\dot{x}(t)$, where $k_{\mathrm{m}} \in \mathbb{R}^{n_{\mathrm{DoF}} \times n_{\mathrm{DoF}}}$ and $b_{\mathrm{m}} \in \mathbb{R}^{n_{\mathrm{DoF}} \times n_{\mathrm{n}}}$ denote the mooring stiffness and damping matrices; (iv) the wave excitation force, represented as $f_{\mathrm{e}}(t) \in \mathbb{R}^{n_{\mathrm{DoF}}}$, denoting the force exerted by the waves; and (v) the PTO control force, expressed as $f_{\mathrm{u}}(t) \in \mathbb{R}^{n_{\mathrm{DoF}}}$.

Note that both the infinite frequency added mass matrix (μ_∞) and the radiation convolution kernel matrix (k_{r}) can be determined based on the frequency-domain radiation added-mass and damping hydrodynamic coefficients ($A_{\mathrm{r}}(\omega) \in \mathbb{R}^{n_{\mathrm{DoF}} \times n_{\mathrm{DoF}}}$ and $B_{\mathrm{r}}(\omega) \in \mathbb{R}^{n_{\mathrm{DoF}} \times n_{\mathrm{DoF}}}$, respectively). This calculation can be performed following Ogilvie's relations [12], which are expressed as follows:

$$\begin{aligned} A_{\mathrm{r}}(\omega) &= \mu_\infty - \tfrac{1}{\omega}\textstyle\int_0^{+\infty} k_{\mathrm{r}}(t)\sin(\omega t)dt, \\ B_{\mathrm{r}}(\omega) &= \textstyle\int_0^{+\infty} k_{\mathrm{r}}(t)\cos(\omega t)dt. \end{aligned} \tag{2}$$

Likewise, the radiation convolution kernel k_{r} can also be defined in the frequency-domain[1], as

$$K_{\mathrm{r}}(\omega) = B_{\mathrm{r}}(\omega) + \jmath\omega\left[A_{\mathrm{r}}(\omega) - \mu_\infty\right]. \tag{3}$$

Hence, Equation (1) can be reformulated in the frequency-domain using the force-to-velocity description [13] as:

$$V(\omega) = Z_i^{-1}(\omega)\left[F_{\mathrm{e}}(\omega) - F_{\mathrm{u}}(\omega)\right], \tag{4}$$

where $Z_i(\omega) \in \mathbb{I}^{n_{\mathrm{DoF}} \times n_{\mathrm{DoF}}}$ denotes the intrinsic impedance of the system, defined as

$$Z_i(\omega) = B_{\mathrm{r}}(\omega) + b_{\mathrm{m}} + \jmath\omega\left(m + A_{\mathrm{r}}(\omega) - \frac{s_{\mathrm{h}} + s_{\mathrm{m}}}{\omega^2}\right). \tag{5}$$

Note that all the hydrodynamic parameters required to define the WEC dynamics (as shown in Eqs. (1) and (4)) can be obtained using standard boundary element method (BEM) solvers, such as Nemoh [14] or WAMIT [15].

Additionally, it's important to highlight that, for simulating the WEC system's motion in the time domain, we approximate the convolution term of the radiation force using a linear time-invariant (LTI) system. This approximation allows us to express Equation(1) in a state-space form, significantly reducing the computational complexity of solving it. This approach is widely used in the literature and various tools are available to obtain the approximation of such a convolution term, such as the FOAMM toolbox [16], [17].

Finally, in this study, we assume that the WEC is tethered to a single pre-tensioned mooring line, with the PTO system linking the buoy to the mooring line. Therefore, the PTO harnesses energy from the relative motion between the buoy and the pre-tensioned mooring line. This configuration aligns with the common approach for near-shore point absorbers, as employed by entities such as the CorPower-C4 device [18].

[1]Denoted by uppercase letters for frequency-domain variables.

III. WEC CONTROL

This section introduces the WEC controller considered in this study. To this end, first, the optimality condition for WECs is introduced in Section III-A, and then the LiTe-Con strategy is described in Section III-B.

A. Optimality condition

For WECs, the energy absorbed (E) within the given time interval $[0,\ T]$, with $T \in \mathbb{R}^+$, can be computed by integrating the converted power as

$$E = -\int_0^T \dot{x}(t) f_{\mathrm{u}}(t) dt. \tag{6}$$

Considering the model defined in Section II, the optimal condition (in terms of $f_u(t)$) for maximum energy absorption can be derived, in the frequency domain, from the impedance-matching problem [13] as

$$F_{\mathrm{u}}(\omega) = -Z^\star(\omega)V(\omega), \tag{7}$$

with $Z^\star(\omega)$ as the complex conjugate of $Z(\omega)$. Additionally, such optimal condition can alternatively be expressed in terms of the optimal velocity profile ($V^{\mathrm{opt}}(\omega)$) as

$$V^{\mathrm{opt}}(\omega) = \frac{1}{Z(\omega) + Z^\star(\omega)}F_{\mathrm{ex}}(\omega) = \frac{1}{2B_{\mathrm{r}}(\omega)}F_{\mathrm{ex}}(\omega), \tag{8}$$

which has purely real mapping and defines a zero-phase-locking condition between the input excitation force $f_{\mathrm{ex}}(t)$ and the velocity of the device [19]. In particular, Eqs. (7) and (8) represent the well-known impedance-matching condition [13]. Note that this condition can be reformulated in a control context as $H_{\mathrm{fb}}(\omega) = Z^\star(\omega)$, defining a feedback (FB) control structure that incorporates the controller $H_{\mathrm{fb}}(\omega)$ within the feedback loop [19]. It is important to note that, while the solution is well-established in WEC control literature, the inherent non-causality of $H_{\mathrm{fb}}(\omega)$ renders it impractical for real-world implementation (the interested reader is referred to [19] for further insights).

When considering such an impedance-matching condition, both the system $G_0(s)$ and the controller $H_{\mathrm{fb}}(s)$ can be represented in the frequency domain as[2]:

$$G_0(s)\Big|_{s=\jmath\omega} = \mathbb{Re}\left(G\right) + \jmath\mathbb{Im}\left(G\right), \tag{9}$$

$$H_{\mathrm{fb}}(s)\Big|_{s=\jmath\omega} = \frac{1}{\mathbb{Re}\left(G\right) - \jmath\mathbb{Im}\left(G\right)}. \tag{10}$$

Thus, the optimal mapping from $F_{\mathrm{ex}}(\omega)$ to $V^{\mathrm{opt}}(\omega)$ (introduced in Equation(8)) can be now described as

$$\frac{V^{\mathrm{opt}}(\omega)}{F_{\mathrm{ex}}(\omega)} = T^{\mathrm{opt}}_{f_{\mathrm{ex}} \to v}(\omega) = \frac{\mathbb{Re}(G)^2 + \mathbb{Im}(G)^2}{2\mathbb{Re}(G)}. \tag{11}$$

[2]For simplicity in notation, let $\mathbb{Re}(G) = \mathbb{Re}\{G_0(\jmath\omega)\}$ and $\mathbb{Im}(G) = \mathbb{Im}\{G_0(\jmath\omega)\}$, which denote the real and imaginary parts, respectively.

B. LiTe-Con strategy

The optimal condition introduced in the previous section (see the mapping from $F_{\text{ex}}(\omega)$ to $V(\omega)$ in Equation(11)) can equivalently be defined with a feed-forward (FF) control structure as

$$H_{\text{ff}}(\omega) = \frac{\mathbb{Re}(G) + \jmath\mathbb{Im}(G)}{2\mathbb{Re}(G)}, \tag{12}$$

where $H_{\text{ff}}(\omega)$ denotes the FF mapping, which is equivalent to the FB structure ($H_{\text{fb}}(\omega)$) introduced in Eq. (10) and, hence, $F_u(\omega) = H_{\text{ff}}(\omega)F_{\text{ex}}(\omega)$.

By means of frequency-domain system identification algorithms, the LiTe-Con strategy approximates such FF mapping $H_{\text{ff}}(\jmath\omega)$ with an LTI dynamical system (denoted as $\tilde{H}_{\text{ff}}(s)$) as:

$$\tilde{H}_{\text{ff}}(s)\Big|_{s=\jmath\omega} \approx H_{\text{ff}}(\omega). \tag{13}$$

Note that, in this case, such approximation is carried out using moment-matching-based identification algorithms [16]. Note that, even though the LiTe-Con strategy proposes a constraint handling mechanism, no physical constraint have been considered in this preliminary study and, hence, it is not introduced here.

IV. Case Study

This section highlights the importance of a comprehensive motion description of the WEC motion when proposing a realistic controller to avoid overestimating power production. To this end, Section IV-A presents the considered WEC system, Section IV-B introduces the studied wave conditions, and Section IV-C details the analysed cases.

A. WEC system

In order to make an analysis with a realistic model, a WEC similar to the CorPower-C4 device [18] is chosen here. The device has an 8 m diameter, with a spherical shape in the middle and conical top and bottom ends. To show the similarities between the considered and real WEC geometry, Fig. 1 shows both the mesh of the considered device (left figure) and a picture of the real CorPower-C4 device (right figure).

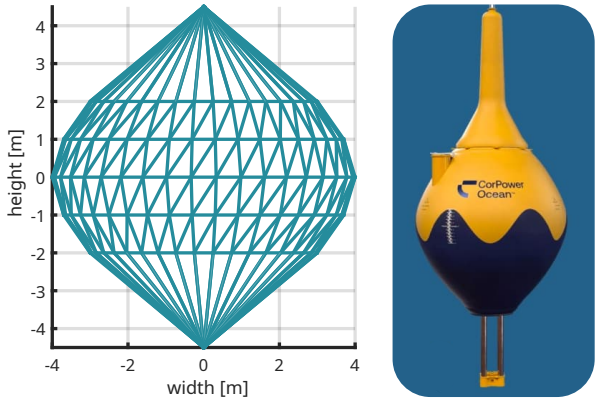

Fig. 1: Mesh of the considered device on the left, and picture of the CorPower-C4 device on the right.

To simplify the analysis, as explained in Section IV-C, only up to 3 DoFs have been considered here: surge, heave, and pitch. The required hydrodynamic coefficients have been obtained using the well-known BEM solver Nemoh [14], from Ecole Centrale de Nantes.

B. Wave conditions

To better comprehend the impact of simplifying the WEC simulation model, all the cases analysed in this study are evaluated with both regular and irregular waves. On the one hand, regular waves offer a basis for comparing the results against theoretically optimal outcomes, as a simple passive-reactive controller can achieve the optimal (unconstrained) performance of a WEC for a single wave frequency. On the other hand, employing irregular waves creates a more realistic scenario, rendering more meaningful results.

For both regular and irregular waves, three different 1000s-long sea states (SSs) have been considered, specified in Table I. In the case of regular waves, sinusoidal waves with period and height as specified on the peak period (T_p) and significant wave height (H_s) columns of Table I are considered; while, on the case of the irregular SSs, waves are generated using a JONSWAP distribution [20], with T_p and H_s as defined in Table I and a peak enhancement factor of 3.3 (which is widely used in the literature).

TABLE I: Parameters of the considered sea states.

	T_p [s]	H_s [m]
SS1 (small waves)	7	1
SS2 (medium waves)	10	2.5
SS3 (large waves)	12	4.5

C. Analysed cases

As mentioned in the introduction, authors usually simplify the model of Equation(1) to consider a single DoF when proposing their controllers. However, in the ocean, it is nearly impossible to completely constrain these DoFs. Therefore, it's crucial to assess how incorporating these additional DoFs in the simulation affects the controller's performance. To this end, from a motion point of view, three test cases (TCs) are analysed here:

- **TC1:** The simulation of the WEC motion is carried out considering a single DoF, heave. This is the most analysed case in the literature, where the DoF of motion of the device coincides with the DoF in which the PTO absorbs energy. Thus, as shown in Fig. 2.a, the motion of the PTO system (x_{m}) is equal to the heave motion of the buoy (z).
- **TC2:** The simulator considers a WEC with two DoFs, surge and heave. In this case, the DoF of the PTO is a function of the two DoFs of the WEC, as shown in Fig. 2.b. The motion of the PTO can be described in this TC as:

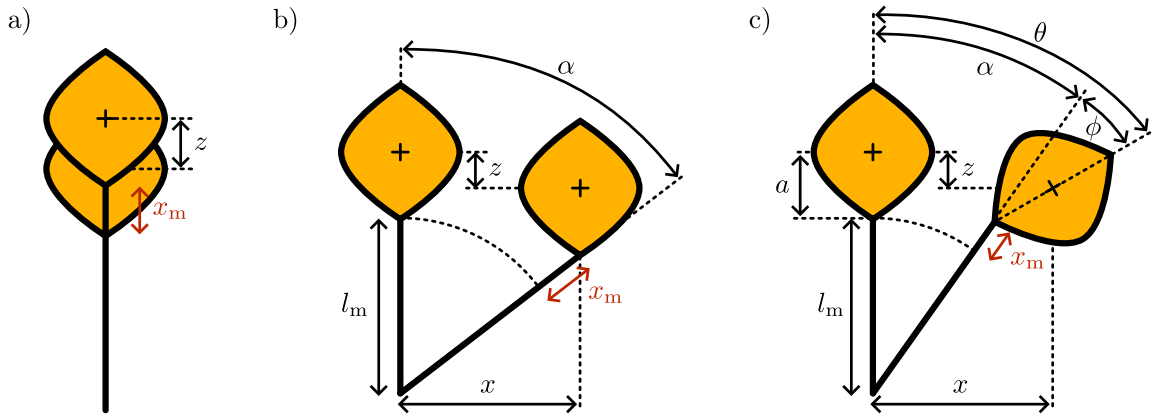

Fig. 2: Diagram of the transformation from the WEC coordinate system to the PTO DoF for the considered TCs.

$$x_m = \sqrt{(z + l_m)^2 + x^2} - l_m,$$
$$\alpha = \tan^{-1}\left(\frac{z + l_m}{x}\right), \tag{14}$$

where l_m is the length of the mooring line.

- **TC3:** The most complex case analysed in this study, where the motion of the device is computed considering three DoFs: surge, heave and pitch. As shown in Fig. 2.c, the definition of the PTO DoF is more complex in this case and can be obtained as [21], [22]:

$$x_m = \sqrt{((l_m + a + z) - a\cos\theta)^2 + (x - a\sin\theta)^2} - l_m,$$
$$\alpha = \tan^{-1}\left(\frac{x - a\sin\theta}{l_m + a + z - a\cos\theta}\right), \tag{15}$$
$$\phi = \theta - \alpha,$$

where a is the distance between the centre of rotation and the mooring connection point.

In addition to the three different TCs addressing device motion introduced before, this study also evaluates two distinct controllers. Firstly, we analyse a common passive-reactive controller without constraints, which aids in computing optimal power in the context of regular waves, providing a reference for the maximum attainable energy in such scenarios. Secondly, we investigate the LiTe-Con strategy, as outlined in Section III-B, which offers a more realistic control approach, suitable for irregular wave conditions. Additionally, within the passive-reactive controller, we explore two distinct approaches. The first approach involves optimising the PTO damping and stiffness coefficients for the motion of the PTO (x_m). Conversely, the second approach focuses on maximising the total energy of the system by optimising PTO damping and stiffness values for each DoF of the WEC. It's important to note that the second approach is highly unrealistic since developing a PTO system able to extract energy from all the DoFs individually in a real scenario would be nearly impossible. Nevertheless, this energy calculation provides an upper limit of the available energy in the system.

Finally, it should be noted that, for the sake of robustness, the power of all cases is determined by calculating the slope of a straight line obtained through a fitting process applied to the cumulative absorbed energy curve. Additionally, in order to avoid the transient behaviour of the WEC at the beginning of the simulations, only the energy absorbed on the last %80 of the simulation time is considered to compute the power (i.e. over the last 800s).

V. Results

This section introduces the results obtained for the case study introduced in Section IV. First, Section V-A shows the results obtained when considering a passive-reactive controller and, then, Section V-B those obtained with the LiTe-Con strategy.

A. Passive-reactive controller

As previously mentioned, in the case of regular waves, it is possible to calculate the optimal power (assuming unconstrained motion) with a simple passive-reactive controller. Furthermore, if we (hypothetically) assume that the PTO system can extract energy from the different DoFs independently (even though this is practically impossible), we can compute the maximum power available for each wave. Fig. 3 illustrates the maximum power available for the three different SSs when considering that the WEC moves in one, two, or three DoFs. It's worth noting that, in general, the total energy increases when considering more DoFs. However, the difference in energy gain becomes less significant when we move to the higher SSs (SS2 and SS3). This phenomenon occurs because, in such SSs, the primary contribution to the total power comes from heave motion, making the contribution from the other two DoFs less prominent.

As expected, the results differ when we consider that the PTO can only operate along a single axis, as explained in Section IV. As depicted in Fig. 4, the most noticeable change is the reduction in power when we account for multiple DoFs. Note that, for the single DoF case, the same power extraction shown in Fig. 3 is achieved. Furthermore, Fig. 4 illustrates the disparity between optimising the PTO damping and stiffness coefficients for heave motion across all TCs versus optimising a unique set of coefficients for each TC. It is evident that the PTO values should be optimised

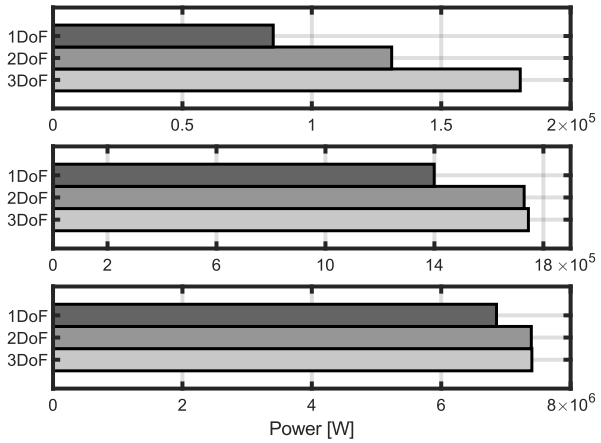

Fig. 3: Absorbed power for the regular SSs (SS1 to SS3, from top to bottom) with the passive-reactive controller, considering that the PTO can absorb energy from the different DoFs separately.

individually for each TC rather than relying solely on those obtained for the primary DoF, which, in this case, is heave.

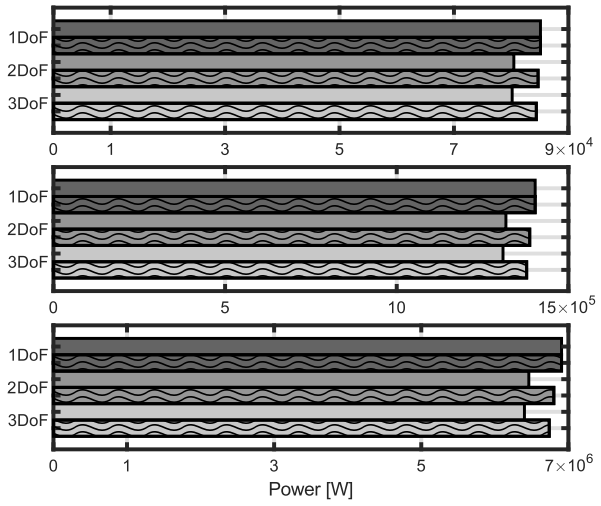

Fig. 4: Absorbed power for the regular SSs (SS1 to SS3, from top to bottom) with the passive-reactive controller, considering the PTO DoF as a combination of the DoFs of the WEC. Cases with the PTO coefficients optimised for such TC are depicted with the wavy pattern.

Finally, when considering irregular waves, similar results to those obtained for the regular SS cases are obtained. By way of example, Fig. 5 shows the absorbed power when the PTO only operates on a single axis, with the PTO coefficients optimised for each TC. As explained before in Fig. 4 for regular waves, the power decreases when considering additional DoFs on the WEC. It should be noted that the decrease on the absorbed power can be attributed to two factors: (i) considering irregular waves, which inherently contain less energy compared to their regular counterparts, and (ii) the limitation of achieving optimal power absorption in the case of irregular SS when using a simple passive-reactive controller.

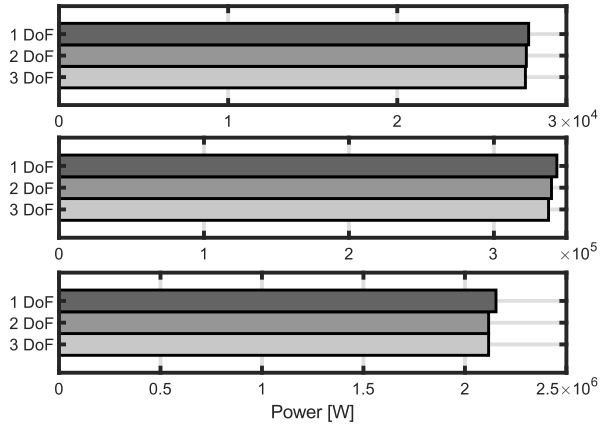

Fig. 5: Absorbed power for the irregular SSs (SS1 to SS3, from top to bottom) with the passive-reactive controller, considering the PTO DoF as a combination of the DoFs of the WEC.

B. LiTe-Con controller

In this section, we present the results achieved using the LiTe-Con controller. Unlike the passive-reactive controller, which allows optimisation of PTO coefficients for any given simulation, the LiTe-Con strategy requires a single-input single-output (SISO) model of the system to describe the controller (as detailed in Section III-B). In this context, and due to the impracticality of characterising the PTO axis with a SISO model (single DoF) across all TCs, the model of the WEC on heave is considered to define the controller.

Figure 6 displays the total absorbed power under regular SSs when employing the LiTe-Con strategy with the PTO operating along a single axis. Comparing these results to those obtained with the passive-reactive controller, shown in Figure 4, it is evident that the LiTe-Con strategy achieves lower power output in this scenario. This discrepancy may be attributed (partially) to the approximation of the dynamical system $\tilde{H}\mathrm{ff}(s)$ at the frequencies corresponding to the considered SSs. However, it should be noted that, if $\tilde{H}\mathrm{ff}(s) = H_{\mathrm{ff}}(s)$, the results for the 1DoF TC should be the same.

Conversely, in the case of irregular waves, the LiTe-Con strategy exhibits superior performance compared to the basic passive-reactive controller, as illustrated in Figure 7 (in contrast to Figure 5), for most scenarios. Notably, for the largest SS (SS3), the LiTe-Con strategy outperforms the passive-reactive controller in the one DoF case, but not for the other two TCs.

Finally, in general, one could notice that, for both regular and irregular SSs, the results obtained with the LiTe-Con strategy mirror the patterns observed with the passive-reactive controller: As the number of DoFs impacting the PTO axis increases, the absorbed power diminishes. This highlights the significance of accounting for all WEC DoFs and employing a realistic representation of the PTO DoF

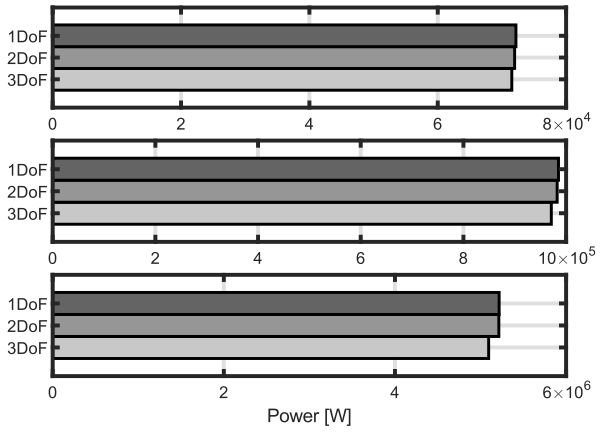

Fig. 6: Absorbed power for the regular SSs (SS1 to SS3, from top to bottom) with the LiTe-Con strategy, considering the PTO DoF as a combination of the DoFs of the WEC.

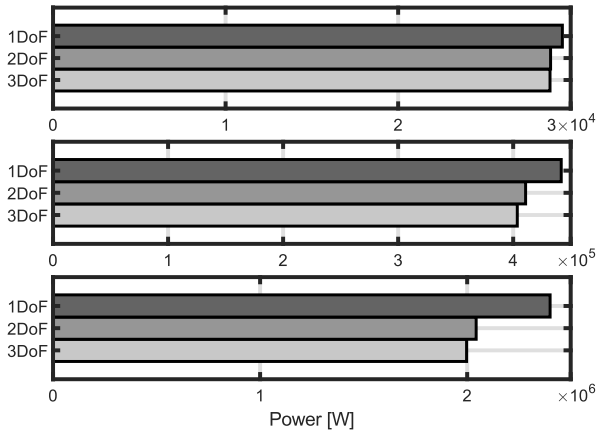

Fig. 7: Absorbed power for the irregular SSs (SS1 to SS3, from top to bottom) with the LiTe-Con strategy, considering the PTO DoF as a combination of the DoFs of the WEC.

during the controller design phase to avoid overly optimistic results.

VI. Conclusions

The current study presents a practical case involving the control of a point absorber wave energy converter (WEC) that can move in one, two, or three degrees of freedom (DoFs). The power take-off (PTO) system of the considered WEC extracts energy from only one DoF, which is the relative motion between the WEC and the pre-tensioned mooring line. The study shows that, in theory, the system should be capable of absorbing more energy when incorporating additional DoFs, given the more extensive motion. However, the application case reveals that, when realistic PTO systems are considered, an increase in the number of DoFs in the WEC description consistently results in reduced absorbed power. Therefore, this study emphasises the significance of accounting for all the DoFs of a WEC and providing an accurate description of the PTO DoF when designing a control strategy to obtain meaningful performance outcomes.

References

[1] IPCC, "Mitigation of climate change. working group iii contribution to the sixth assessment report of the intergovernmental panel on climate change," Intergovernmental Panel on Climate Change (IPCC), Tech. Rep. ISBN 978-92-9169-160-9, 2022.

[2] Stéphanie Bouckaert, A. F. Pales, C. McGlade, U. Remme, and B. Wanner, "Net Zero by 2050: A Roadmap for the Global Energy Sector," International Energy Agency, Paris, Tech. Rep., 2021.

[3] Ocean Energy Europe, "2030 Ocean Energy Vision," Tech. Rep., 2020. [Online]. Available: https://www.oceanenergy-europe.eu/wp-content/uploads/2020/10/OEE_2030_Ocean_Energy_Vision.pdf

[4] NREL, "Marine Energy in the United States : An Overview of Opportunities," Tech. Rep. February, 2021. [Online]. Available: https://www.nrel.gov/docs/fy21osti/78773.pdf

[5] K. Wang, Z. Wang, S. Sheng, Y. Zhang, Z. Wang, Y. Ye, W. Wang, H. Lin, and Z. Huang, "A method for large-scale wec connecting to island isolated microgrid based on multiple small power hpgss," *Renewable Energy*, p. 119330, 2023.

[6] F. Fusco, G. Nolan, and J. V. Ringwood, "Variability reduction through optimal combination of wind/wave resources–an irish case study," *Energy*, vol. 35, no. 1, pp. 314–325, 2010.

[7] S. Astariz and G. Iglesias, "Output power smoothing and reduced downtime period by combined wind and wave energy farms," *Energy*, vol. 97, pp. 69–81, 2016.

[8] W. Sasaki, "Predictability of global offshore wind and wave power," *International journal of marine energy*, vol. 17, pp. 98–109, 2017.

[9] B. Guo and J. V. Ringwood, "A review of wave energy technology from a research and commercial perspective," *IET Renewable Power Generation*, vol. 15, no. 14, pp. 3065–3090, 2021.

[10] J. V. Ringwood, S. Zhan, and N. Faedo, "Empowering wave energy with control technology: Possibilities and pitfalls," *Annual Reviews in Control*, 2023.

[11] S. Zou, O. Abdelkhalik, R. Robinett, U. Korde, G. Bacelli, D. Wilson, and R. Coe, "Model predictive control of parametric excited pitch-surge modes in wave energy converters," *International journal of marine energy*, vol. 19, pp. 32–46, 2017.

[12] T. F. Ogilvie, "Recent progress toward the understanding and prediction of ship motions," in *5th Symposium on Naval Hydrodynamics*, vol. 1. Bergen, Norway, 1964, pp. 2–5.

[13] J. Falnes, *Ocean Waves and Oscillating Systems: Linear Interactions Including Wave-Energy Extraction*. Cambridge Univ. Press, 2002.

[14] M. Penalba, T. Kelly, and J. Ringwood, "Using nemoh for modelling wave energy converters: A comparative study with wamit," in *12th European Wave and Tidal Energy Conference (EWTEC)*, 2017.

[15] WAMIT, "Wamit," https://www.wamit.com, 2023, online accessed 24-Oct-2023.

[16] N. Faedo, Y. Peña-Sanchez, and J. V. Ringwood, "Finite-order hydrodynamic model determination for wave energy applications using moment-matching," *Ocean Engineering*, vol. 163, pp. 251–263, 2018.

[17] Y. Pena-Sanchez, N. Faedo, M. Penalba, G. Giuseppe, A. Mérigaud, C. Windt, D. G. Violini, W. LiGuo, and J. Ringwood, "Finite-order hydrodynamic approximation by moment-matching (foamm) toolbox for wave energy applications," in *European Tidal and Wave Energy Conference Proceedings*, vol. 2019, no. 1448. EWTEC, 2019.

[18] CorPower Ocean, "CorPower website," https://corpowerocean.com/, 2023, online accessed 24-Oct-2023.

[19] D. García-Violini, Y. Peña-Sanchez, N. Faedo, and J. V. Ringwood, "An energy-maximising linear time invariant controller (LiTe-Con) for wave energy devices," *IEEE Transactions on Sustainable Energy*, vol. 11, no. 4, pp. 2713–2721, 2020.

[20] K. Hasselmann, "Measurements of wind wave growth and swell decay during the Joint North Sea Wave Project (JONSWAP)," *Deutches Hydrographisches Institut*, vol. 8, p. 95, 1973.

[21] B. W. Schubert, W. S. Robertson, B. S. Cazzolato, and M. H. Ghayesh, "Linear and nonlinear hydrodynamic models for dynamics of a submerged point absorber wave energy converter," *Ocean Engineering*, vol. 197, p. 106828, 2020.

[22] B. W. Schubert, W. S. Robertson, B. S. Cazzolato, N. Y. Sergiienko, and M. H. Ghayesh, "Nonlinear stiffness enhancement of submerged wave energy device in high fidelity model," *Ocean Engineering*, vol. 254, p. 111295, 2022.